Acta Materialia 219 (2021) 117251

Contents lists available at ScienceDirect

Acta Materialia

journal homepage: www.elsevier.com/locate/actamat

Full length article

Influence of graded doping on the long-term reliability of Nb-doped lead zirconate titanate films

Wanlin Zhu[a,*], Betul Akkopru-Akgun[a], Jung In Yang[a], Charalampos Fragkiadakis[b,1], Ke Wang[a], Song Won Ko[b], Peter Mardilovich[b,1], Susan Trolier-McKinstry[a]

[a] Materials Research Institute and Department of Materials Science and Engineering, Pennsylvania State University, 16802, USA
[b] Xaar plc, Cambridge CB4 0XR, UK

ARTICLE INFO

Article history:
Received 29 April 2021
Revised 26 July 2021
Accepted 11 August 2021
Available online 24 August 2021

Keywords:
Long-term reliability
PZT films
Graded doping
Conduction mechanism
Transmission electron microscopy electron energy loss spectroscopy

ABSTRACT

Niobium doped lead zirconate titanate (PNZT) films show potential in piezoelectric microelectromechanical systems (piezoMEMS); their long-term reliability is important for successful application. This work describes how variations in the doping profile through the film depth can significantly increase the long-term reliability of PNZT films, while retaining excellent piezoelectric properties. Chemical solution derived {100} textured PNZT films were prepared with a Mn-doped lead zirconate titanate (PMZT) layer at the film top or bottom surface (PNZT + x mol% PMZT, or x mol% PMZT + PNZT). No significant differences were found in the baseline dielectric, ferroelectric and piezoelectric properties of the films. As the Mn-doping concentration increased, the medium time to failure (t_{50}) of PNZT + x mol% PMZT and x mol% PMZT + PNZT films gradually increased from 14.4 h to 93.9 hours, and from 27.7 to 94.6 hours, respectively, under aggressive test conditions (200°C, 300 kV/cm) where the Mn doped layer served as the cathode. Current – voltage measurement on pristine PNZT + 2 mol% PMZT films showed Schottky emission-controlled conduction. After a 23 hours degradation period at 200°C, 300 kV/cm (field up), Poole-Frenkel conduction became dominant. The trap energy level increased from 0.45 ± 0.01 eV for PNZT to 1.27 ± 0.03 eV for the PNZT + 2 mol% PMZT film. Furthermore, Ti^{4+} reduction was found in degraded PNZT near the top electrode, but not in degraded PNZT + 2 mol% PMZT, as recorded by electron energy loss spectroscopy data. Electron trapping by Mn ions showed strong contributions to suppression of the conduction and improvement of long-term reliability for the PNZT film with a PMZT (top or bottom) layer.

1. Introduction

Lead zirconate titanate films with compositions near the morphotropic phase boundary ($Pb(Zr_{0.52}Ti_{0.48})O_3$, PZT) are widely utilized in microelectromechanical systems (MEMS), including actuators [1], ultrasonic transducer arrays [2], and inkjet printer heads [3]. In MEMS applications, both the piezoelectric properties and long-term reliability depend on the defect chemistry and crystallographic orientation of the films. Much of the published literature [4-6] shows that {100}-oriented PZT films display a higher transverse piezoelectric coefficient $e_{31,f}$, compared to films of the same composition with either random or {111} orientation. In addition, donor doping of PZT with ions like Nb on the B site has been shown to increase the electrical resistivity [7], increase the mobility of domain walls [8], decrease the oxygen vacancy concentration [9,10], and minimize local stresses [11], thus increasing the piezoelectric response [12]. In contrast, acceptor doping raises both the oxygen vacancy and the hole concentration (and hence the electrical conductivity), provides local electric fields associated with defect dipoles such as $Mn''_{Ti} - V_O^{\bullet\bullet}$, $Fe'_{Ti} - V_O^{\bullet\bullet}$ [13,14], and reduces the mobility of domain walls [15,16], producing smaller but more stable [7] piezoelectric coefficients.

PZT is normally a p-type semiconductor due to loss of Pb during sample preparation [17], with an n-type interface due to oxygen vacancy formation at the surfaces [18,19]. The leakage current of PZT films is often controlled by Schottky emission at the electrode/PZT interface as a result of this n-type layer [20]. In some cases, transitions between conduction mechanisms develop as a function of the applied electric field [21]; the details of this are expected to vary with the doping type, doping concentration and degradation states.

In many electroceramics, including $Pb(Zr,Ti)O_3$ and $BaTiO_3$, oxygen vacancy migration controls the long-term reliability under DC

* Corresponding author.
E-mail addresses: wuz14@psu.edu, wanlinzhu0927@gmail.com (W. Zhu).
[1] Current affiliation: aixACCT System GmbH, Talbotstr. 25, 52068 Aachen, Germany.

https://doi.org/10.1016/j.actamat.2021.117251
1359-6454/

electric fields. For example, Waser et al. [22-24] reported that oxygen vacancy migration towards the cathode side is a primary cause of resistance degradation. Warren et al. determined that for $BaTiO_3$, motion of oxygen vacancies within the oxygen octahedron had an activation energy of 0.9 eV [25]. Long-range motion of oxygen vacancies typically has an activation energy of ~0.6 eV in PZT [26]. The long-term reliability (lifetime) of PZT films is affected by their defect population, doping, interface asymmetry, and charged point defect trapping, and migration of both electronic and ionic species [27,28], including oxygen vacancies, $V_O^{\bullet\bullet}$ [15,29]. It was recently demonstrated that the lifetime of PZT films under DC electric field is mainly governed by the long-range migration of oxygen vacancies, with associated changes in the film-electrode interface state [21].

Many researchers claimed that donor doping of perovskites reduces resistance degradation by reducing the concentration of oxygen vacancies. In contrast, acceptor doping tends to increase the degradation rate in ferroelectric materials like $BaTiO_3$ and $Pb(Zr,Ti)O_3$ due to the higher initial concentration of oxygen vacancies [30–32]. Intriguingly, however, Akkopru-Akgun et al. [21,33] observed higher lifetimes under highly accelerated lifetime testing (HALT) conditions in Mn-doped PZT films, relative to donor doped films. It was hypothesized that multi-valent Mn ions allow electron or hole trapping, resulting in improved resistance degradation behavior and lifetimes of Mn doped PZT films. Eichel [34] confirmed the existence of $Mn''_{Ti} - V_O^{\bullet\bullet}$ defect complexes in $PbTiO_3$; multiple oxidation states for the Mn ions also provided trapping centers for electrons.

In this study, PZT films with graded doping concentrations were studied to understand whether it is possible to prepare films which combine high piezoelectric properties and excellent long-term reliability. The intent was to utilize donor doped films for their high piezoelectric responses, with a thin layer of Mn-doped material to increase the lifetime. Both the location of the Mn-doped layer in the stack and the concentration of Mn were varied so that the effect of this layer on the functional properties could be assessed. The $d_{33,f}$ and median time to failure (t_{50}) was measured by a highly accelerated lifetime test (HALT) to characterize the effect of different doping sequences on the piezoelectric response and long-term reliability. Based on the conduction mechanism analysis, transmission electron microscopy (TEM), electron energy loss spectroscopy (EELS), a working model of the lifetime in PZT films with a graded doping profile was developed.

2. Experimental procedure

To study the influence of a graded doping layer on the long-term reliability of Nb-doped PZT (PNZT) films, two sets of samples were prepared: (1) PNZT films covered by a Mn-doped PZT (PMZT) layer with different Mn doping concentrations; (2) PNZT films grown on a PMZT seed layer with different Mn doping concentrations. The commercial chemical solutions (PZT-E1, Mitsubishi Materials Corporation, Tokyo, Japan) used for the seed layer, bulk layer and top layer are shown in Table 1. For all films, Si wafers with a 30 nm TiO_2 adhesion layer and 150 nm Pt deposited at elevated temperatures were utilized.

~60 nm thick Ti-rich PNZT or PMZT seed layers were used to minimize formation of any pyrochlore phase [28,35-37] and facilitate strong {100} orientation of the films. The seed layers were spin coated at 3500 rpm for 45 sec., pyrolyzed at 200°C for 150 sec, and then crystallized at 700°C for 60 sec. with 2 slpm O_2 flow and 10°C/sec. ramp rate in a rapid thermal annealer (AccuThermo AW 810 RTP, Allwin21 Corp.). After the seed layer, PNZT bulk layers with 2 mol% Nb were prepared by spinning the solutions at 2750 rpm for 45 sec. The films were then pyrolyzed sequentially at 100°C for 60 s and 300°C for 240 s, crystallized at 700°C using the same conditions as for the seed layer. The process was subsequently repeated to build up the bulk of the film. The PMZT top layer was prepared by a process similar to that used in the PNZT bulk layer, except with a 4500 rpm spin-coating speed, resulting in a film thickness ~ 60 nm. The films final thickness are shown in Table 2.

Table 1
PZT E-1 chemical solutions used for film deposition.

Deposition for	Composition
Seed Layer	12wt.% $Pb_{1.20}(Zr_{0.44}Ti_{0.56})_{0.98}Nb_{0.02}O_{3.2}$
	12wt.% $Pb_{1.19}(Zr_{0.44}Ti_{0.56})_{0.99}Mn_{0.01}O_{3.19}$
	12wt.% $Pb_{1.20}(Zr_{0.44}Ti_{0.56})_{0.98}Mn_{0.02}O_{3.2}$
Bulk Layer	15wt.% $Pb_{1.14}(Zr_{0.52}Ti_{0.48})_{0.98}Nb_{0.02}O_{3.14}$
Top Layer	15wt.% $Pb_{1.13}(Zr_{0.52}Ti_{0.48})_{0.99}Mn_{0.01}O_{3.13}$
	15wt.% $Pb_{1.14}(Zr_{0.52}Ti_{0.48})_{0.98}Mn_{0.02}O_{3.14}$
	15wt.% $Pb_{1.15}(Zr_{0.52}Ti_{0.48})_{0.97}Mn_{0.03}O_{3.15}$

X-ray diffraction (XRD, Empyrean & X'Pert pro MPD, PANalytical, Almelo, The Netherlands, Cu$K\alpha$ radiation), and Field Emission Scanning Electron Microscopy (FE-SEM, Merlin & Sigma, ZEISS, Oberkochen, Germany) were employed to check the phase, orientation, and microstructure. (Supplemental materials)

For electrical characterization, an array of 100 nm thick platinum top electrodes with a diameter of 0.5 mm were deposited by RF-sputtering and patterned through a standard lift-off process. Films were post annealed in air for 60 sec. at 550°C to improve the interface adhesion between the film and Pt electrode prior to electrical measurements. The relative permittivity and dielectric loss of the films were measured using an LCR meter (Hewlett Packard 4284A, Palo Alto, USA) from 1 kHz to 1 MHz with a 30 mV AC signal. The polarization-electric field hysteresis loops (P-E loop) were collected using a Multiferroics Analyzer (Radiant Technologies, Albuquerque, USA) with a 100 Hz ac signal and a 400 kV/cm maximum field. Before the piezoelectric measurements, the films were poled at 150 kV/cm for 20 min at 150°C. Two polarities were used for the poling study: field up (the electric field is directed towards the top electrode) and field down (the electric field is directed towards the bottom electrode). A double beam laser interferometer (aixDBLI, aixACCT Systems, Aachen, Germany) was used to obtain both the remanent piezoelectric coefficient (measured at zero DC field from the decreasing field arm of the $d_{33,f}$ loop measurement from 0 to 100 kV/cm with a superimposed 500 mV, 1 kHz ac signal) and the large signal $d^*_{33,f}$ under a 100 Hz 100 kV/cm triangular waveform signal. 0.5 mm circular top electrodes (1.25:1 diameter: substrate thickness ratio) were used to obtain the piezoresponse measurements, eliminating the effects of Poisson's ratio of the substrate on the measurements [38,39,55].

For HALT measurements, the films were cleaved into 7 mm × 7 mm pieces and adhered to a 24-pin DIP package using silver epoxy. The top electrodes were wire bonded to the contact pads of the DIP package with Au wire. A Keithley picoammeter was used as the DC source and leakage current measurement tool. Labview based software monitored the leakage current across the films as a function of the time under HALT degradation conditions (200°C, with 300 kV/cm electric field applied).

The leakage current of the films was measured using a 4140B Hewlett-Packard Agilent pA meter, Santa Clara, CA at varying temperatures (room temperature to 250°C), for conduction mechanism analysis. The pA meter combined with a high temperature DIP package socket was used to record current-voltage (I-V) measurements at different temperatures for PNZT and PNZT with top and bottom 2 mol% PMZT before and after degradation. In all cases a stabilization time of 60 sec was used before the leakage current

Table 2
PNZT films with/without graded doping layer.

Top graded doping layer		Bottom graded doping layer	
Film	Thickness (μm)	Film	Thickness (μm)
PNZT	~1.50	PNZT	~1.50
PNZT + 1 mol% PMZT	~1.56	1 mol% PMZT + PNZT	~1.55
PNZT + 2 mol% PMZT	~1.56	2 mol% PMZT + PNZT	~1.52
PNZT + 3 mol% PMZT	~1.56		

measurement was taken. The piezoresponse, HALT t_{50}, and leakage current were measured in two polarities: field up and field down.

Modulus spectroscopy[40] was performed using a Solartron Analytical Modulab XM (Oak Ridge, USA). Films in both pristine and degraded states were heated up to a series of constant temperature from 180°C to 340°C, and were then measured using a 100 mV AC signal from 1MHz to 1mHz.

Transmission electron microscopy (TEM) and high-angle annular dark-field (HAADF) scanning transmission electron microscopy (STEM) were performed at 200 kV using a FEI dual aberration corrected scanning/TEM (S/TEM). After a thick protective amorphous carbon layer was deposited, cross-sectional TEM specimens were prepared by an in situ milling and lift-out procedure in a focused ion beam (FIB, Helios NanoLab DualBeam 660, FEI Company, Hillsboro, OR). To minimize damage and thin the specimen to electron transparency, the FIB-TEM membrane was fabricated using an initial milling accelerating voltage of 30 kV which was then stepped down to 2 kV.

Ti valence states for the PNZT and PNZT with top 2 mol% PMZT films before and after degradation were studied using electron energy loss spectroscopy (EELS) in STEM mode. A GIF Quantum 963 system was used to collect all the EELS data. By using a X-FEG high brightness electron gun with a monochromator, the energy resolution was ~0.1 eV. EELS spectra were collected using a beam-defining aperture (C2 aperture) size of 70 μm, camera length of 38 mm, entrance aperture of 2.5 mm, and a dispersion of 0.1 eV/pixel. This corresponds to convergence and collection semi-angles of 9.3 and 18.7 mrad, respectively.

3. Results and discussion

As shown in Fig. 1 (a), the low field permittivity and dielectric loss are weakly frequency dependent from 1 kHz to 1 MHz. All films show a similar permittivity around 1500 and a loss tangent close to ~0.02 at 1 kHz (Fig. 1 (a), (b)). No significant change was found in response to the Mn doping concentrations in the top or bottom layer. Fig. 1 (c) and (d) show a group of well saturated polarization-electric field loops (P-E loops) in PNZT and PNZT films with Mn doped top or bottom layers, measured at 400 kV/cm. For the PNZT with 1, 2 and 3 mol% Mn doped top layer films, the remanent polarization P_r was 14 ± 0.4, 14 ± 0.5, and 15 ± 0.2 μC/cm^2, and the coercive field E_c was about 25 ± 0.6 kV/cm. For 1 and 2 mol% Mn doped bottom layers, the P_r was 15 ± 0.4, 14 ± 0.3 μC/cm^2, and E_c was ~ 27 ± 0.5 kV/cm. The Pr and Ec for PNZT films with a Mn-doped near either the top or bottom electrode are essentially identical to the values for PNZT films (P_r = 13 ± 0.5 μC/cm^2, 24 ± 0.3 kV/cm).

A poling study was done for all six films; Fig. 2 presents the piezoelectric properties of the films with the graded doping concentrations. No significant differences were found in either the remanent $d_{33,f}$ or the large signal $d^*_{33,f}$ based on the Mn doping concentration of the top layer. Similarly, no obvious changes were found in the large signal $d^*_{33,f}$ as a function of the Mn doping concentration of the bottom layer, although the remanent $d_{33,f}$ slightly increased as the Mn doping concentration increased in the bottom layer. Thus, although Mn-doped PZT films typically show comparatively smaller piezoelectric coefficients than donor doped films [7,14], since the volume of the film that was Mn doped here was small, there was no adverse effect on the actuator properties. To maintain good piezoelectric response, the Mn doping concentration was limited up to 3 mol%.

To assess the lifetime of PNZT with/without a graded doping layer, HALT measurements were done on all six films under aggressive conditions (300 kV/cm, 200°C). The time dependence of the leakage current density (J_{cap}) was measured for degradation in both field up and field down polarities. A sample population of more than 20 capacitors was used for each HALT measurement. The failure time for each capacitor was defined as the time the J_{cap} increased two orders of magnitude with respect to the minimum leakage current density value. The time at which 50% of the capacitors failed was defined as the median time to failure (t_{50}) [41,42].

Fig. 3 shows the effect of Mn doping concentration on t_{50} for PNZT films with top or bottom graded doping layers. For field up measurements, t_{50} increased from 14.4 to 34.7 to 65.0 to 93.8 hours as the top layer Mn doping concentration increased from 0, 1, 2, to 3 mol%. There was no change in t_{50} with an increase in bottom layer Mn doping concentration for HALT measurements in the field up configuration. When in the field down configuration, there was no consistent change in t_{50} in films with a top Mn doped layer. However, in films with a bottom Mn doped layer t_{50} increased significantly from 27.2 to 68.1 to 94.6 hours with an increase in Mn doping concentration. Thus, the long-term reliability of the films showed a substantial increase when the Mn doped layer appeared on the cathode side. The lifetime increased further as the Mn concentration of this layer rose from 0 to 3 mol%. There are multiple additional potential sources for asymmetry in the HALT lifetimes, including Zr/Ti gradients [21] and gradients in the lead or oxygen vacancy concentration [21]. As shown in Table 3, these factors may be responsible for the field dependence of the HALT lifetimes for PNZT films without a Mn layer. It is important to note, though, that the addition of a Mn layer leads to significantly greater polarity dependence to the HALT lifetimes, and produces higher absolute lifetimes as well.

In order to assess whether the significant improvement in long-term reliability of PNZT films with a PMZT layer on the cathode side implied a change in the interface related conduction mechanism, the conduction mechanism of these films in pristine and degraded states was investigated by three different methods: temperature dependence leakage current measurements, imaginary modulus spectroscopy and STEM EDS and EELS investigation. A PNZT film with 2 mol% PMZT top layer was used for this study.

The leakage current was measured at different temperatures, field polarities (field up or field down) and degradation states (pristine or degraded state). Schottky emission (Eq. 1) and Poole Frenkel conduction (Eq. 2) were found to be the dominant mechanisms, respectively, in pristine and degraded PNZT with a 2 mol% PMZT top layer film [6,43,44]:

Schottky (interface controlled)

$$J_s = AT^2 exp\left[\frac{-q\phi_B + \sqrt{q^3E/4\pi\varepsilon_0\varepsilon_i}}{kT}\right] \quad (1)$$

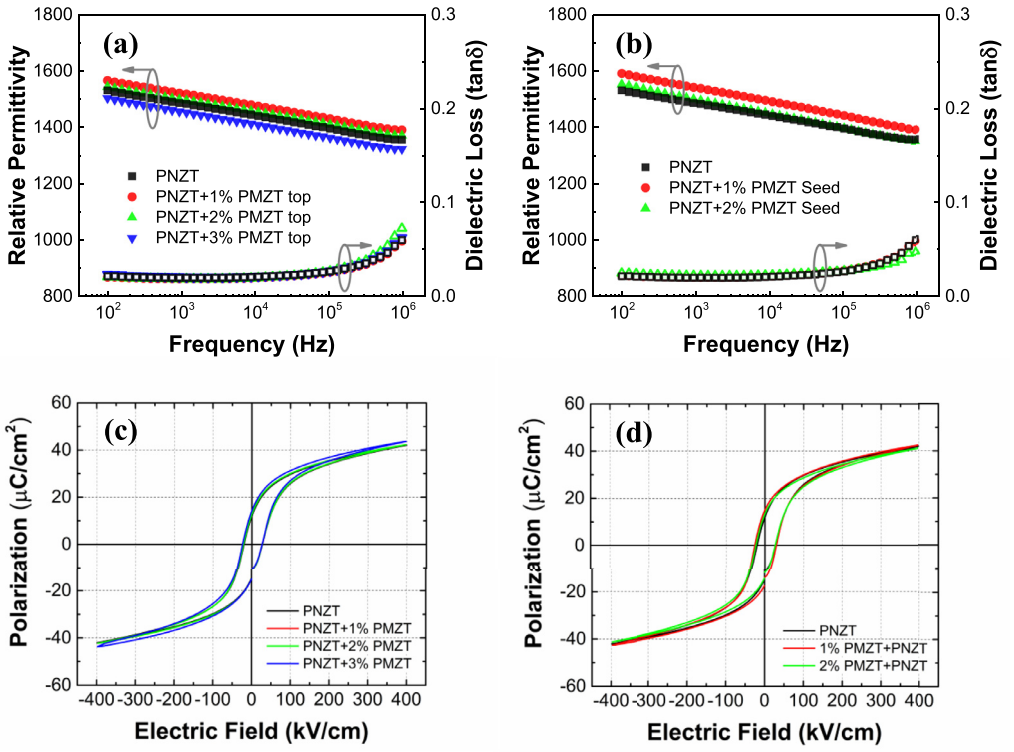

Fig. 1. Mn doping concentration dependence of permittivity (a), (b), and polarization-electric field hysteresis loops (c), (d) for the films with top PMZT and bottom PMZT layer, respectively.

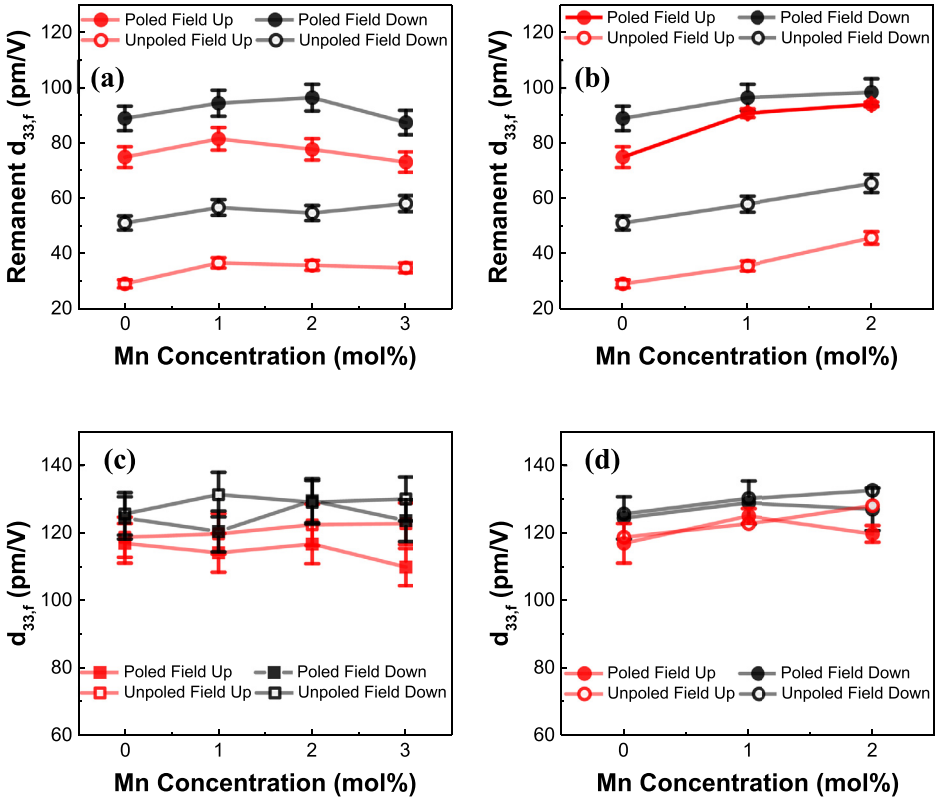

Fig. 2. Mn doping concentration dependence of remanent and large signal $d^*_{33,f}$ of the PNZT films with (a) (c) top PMZT and (b) (d) bottom PMZT layer, respectively.

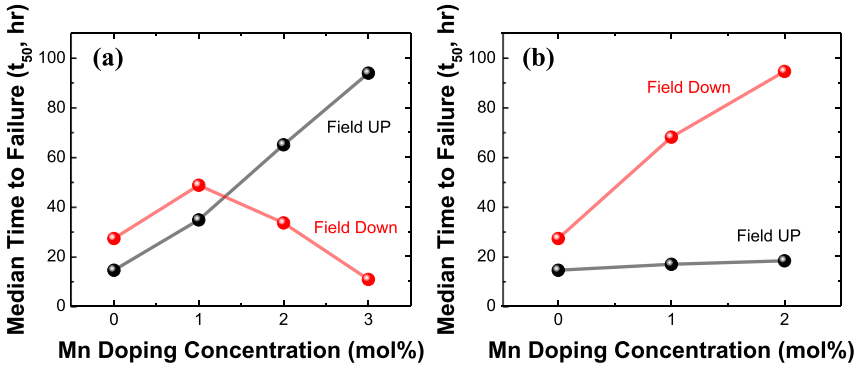

Fig. 3. Dependence of t_{50} on the Mn doping concentration of PNZT films with (a) a top PMZT layer and (b) a bottom PMZT layer.

Table 3
Median time to failure of PNZT films with/without graded doping layer.

Film	t_{50} (hours)		Film	t_{50} (hours)	
	Field Up	Field Down		Field Up	Field Down
PNZT	14.4	27.2	PNZT	14.4	27.2
PNZT + 1 mol% PMZT	34.7	48.7	1 mol% PMZT + PNZT	16.8	68.1
PNZT + 2 mol% PMZT	65.0	33.5	2 mol% PMZT + PNZT	18.2	94.6
PNZT + 3 mol% PMZT	93.9	10.7			

Poole-Frenkel (bulk controlled)

$$J_{pf} = q\mu N_C \mathrm{E}\ \exp\left[-\frac{q\phi_T}{kT} + \frac{q\sqrt{qE/\pi\varepsilon_i\varepsilon_0}}{kT}\right] \quad (2)$$

where J is the current density, q is the electronic charge, μ is the electronic drift mobility, Nc is the density of states in the conduction band, E is the electric field, k is the Boltzmann's constant, T is the temperature, A is the effective Richardson constant, $q\phi_B$ is the Schottky barrier height, $q\phi_T$ is the trap energy level of Poole Frenkel conduction, ε_0 is the permittivity in vacuum, and ε_i is the optical dielectric constant.

It was found that Schottky emission was the dominant conduction mechanism in pristine state films from 100°C to 250°C for both polarities. For the PNZT and PNZT films with 2 mol% PMZT top layer, the Schottky barrier height (SBH) varied around 0.62 ± 0.09 eV in the field up measurements, and increased from 0.46 ± 0.03 to 0.69 ± 0.04 eV in the field down measurements, as the Mn concentration in the top layer increased.

It is hypothesized that the anisotropy in Schottky barrier height for the PNZT films arises from a gradient in the lead content. That is, there are more V''_{Pb} near the top interface (caused by using a lead-rich seed layer, coupled with loss of lead from the top surface of the films during crystallization). This produces a lead gradient which would be expected to be opposite of that of the films reported by Akkopru-Akgun et al. [21,33]. Their films should have more V''_{Pb} near the bottom interface (because in that case the films were prepared using a PbO capping layer on the top surface after the last PNZT crystallization step; there was no additional lead introduced near the substrate). It is notable that they report the opposite anisotropy in the Schottky barrier height with voltage polarity for their films relative to this work. The location of the V''_{Pb} rich region (top surface or bottom interface of the films) significantly contributed to the different trends of these two sets of SBH values. Also, these very different SBH values compared to the values reported by Akkopru-Akgun et al. [21,33], could strongly dominated by the possible very different defect populations and distribution in those films, which were made by different solution with different pyrolysis steps and crystallization environment.

After 23 hours of degradation with 300 kV/cm electric field applied at 200°C, in both PNZT and PNZT + 2 mol% PMZT films, Poole-Frenkel conduction became the dominant mechanism, rather than Schottky emission. The trap energy level for these two films in the field down direction was 0.65 ± 0.05 eV and 0.59 ± 0.03 eV, respectively. In field up measurements, the trap energy level for PNZT was 0.45 ± 0.01 eV, similar to the values found in the field down direction. However, in the field up direction PNZT + 2 mol% PMZT trap energy levels were 1.27 ± 0.03 eV, almost two times higher than the field down direction. This result implied that the added Mn-doped layer of this film became dominant. In PZT, V''_{Pb} and $V_O^{\bullet\bullet}$ are the main types of ionic defects. $V_O^{\bullet\bullet}$ can migrate [29] in PZT under DC voltage towards the cathode side, leaving V''_{Pb} at the anode side. For charge compensation of the ionic defects, electrons and holes accumulate around the PZT cathode and anode regions, respectively. The electrons are trapped by the Ti^{4+} ion, causing reduction to Ti^{3+} (Eq 3) [45].

$$Ti^{4+} + e' \rightarrow Ti^{3+} \quad (3)$$

This is confirmed by the STEM EELS data. The difference, Δ, between the positions of the Ti L_3 edges was defined as (Eq. 4):

$$\Delta = P(e_g) - P\left(t_{2g}\right) \quad (4)$$

$P(e_g)$: is the e_g edge energy $P(t_{2g})$: is the t_{2g} edge energy. Fig. 4 (a) (b) shows Δ values for the top to bottom of PNZT and PNZT + 2 mol% PMZT films before and after 23 hours degradation at 200°C and 300 kV/cm (field up polarity). In degraded PNZT films, the layer contacting the cathode (top electrode) after degradation showed a smaller Δ compared to the layer underneath, or to the same position in pristine PNZT films.

In contrast, in the degraded PNZT + 2 mol% PMZT film, Δ at the cathode interface was slightly larger than was found for the position underneath or for the PNZT films (See Fig. 4 (c) and (d)). Yang et al. showed that Δ is reduced when Ti^{4+} is reduced to Ti^{3+} in $BaTiO_3$ multilayer ceramic capacitors close to the Ni inner electrode, due to the low oxygen content in that region [46,47]. Therefore, the smaller Δ in the top layer of degraded PNZT implies that there are electrons trapped on some of the titanium sites.

It is notable that Δ is unchanged in PNZT + 2 mol% PMZT films, which experience similar aggressive degradation as for the

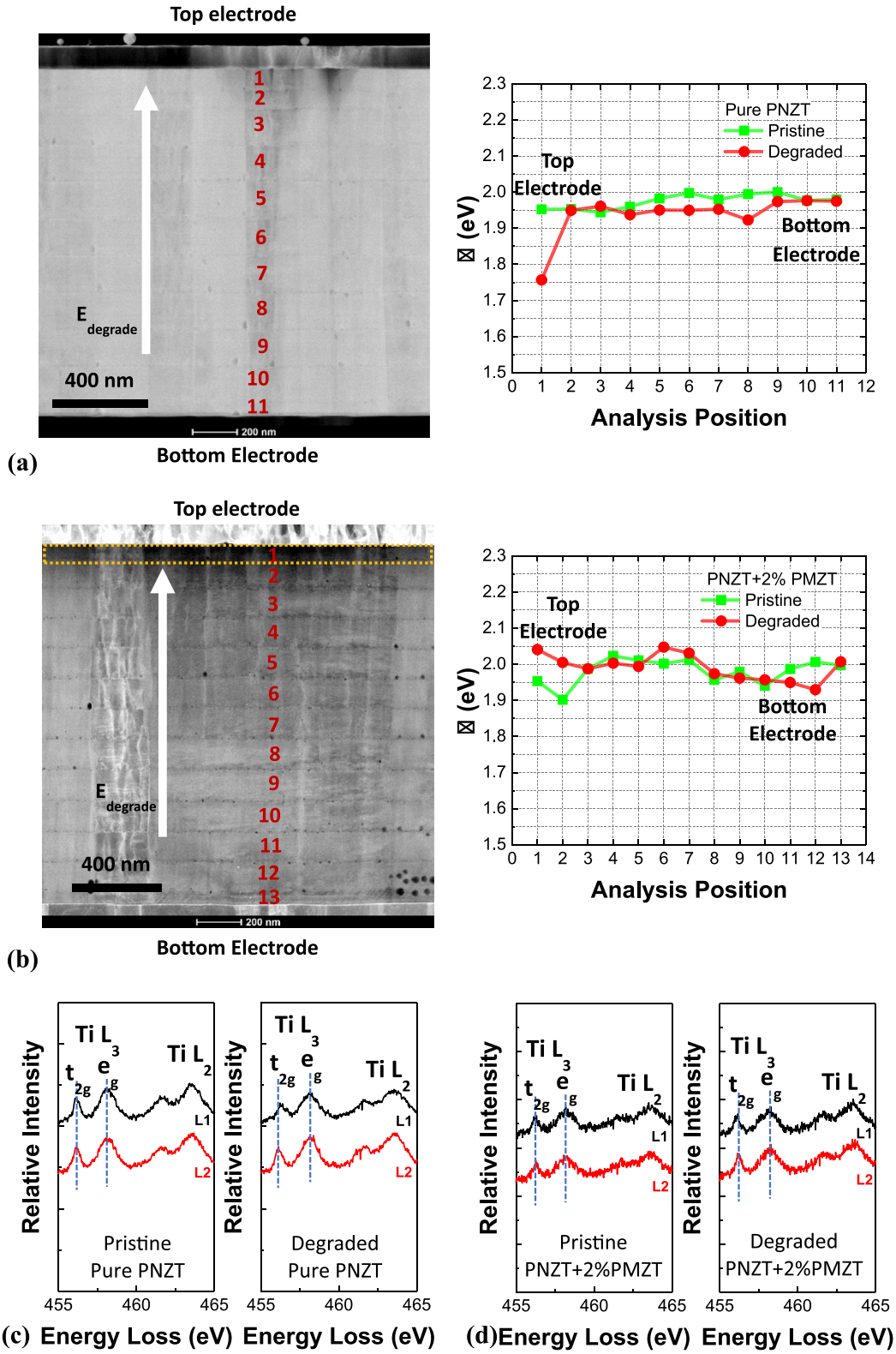

Fig. 4. TEM EELS Δ before and after degradation of pure PNZT and PNZT + 2% PMZT (a) (b) layer by layer (Δ = edge position difference between the e_g and t_{2g} of the Ti L_3 edges); (c) (d) comparison of EELS signals at positions 1 and 2. (The dot rectangle box in TEM HAADF cross-section images in (b) marked the 2 mol% Mn doped PZT layer).

PNZT films. The only explanation is that the electrons are trapped elsewhere. Mn ions have multiple valence states, like Mn^{2+}, Mn^{3+}, Mn^{4+} [22,48,49], and can act as charge trapping centers in PZT films. Due to lower energy levels in the band gap [50], the injected electrons are trapped more easily by Mn than Ti ions in PZT. Therefore, no obvious Ti ion reduction in degraded PNZT + 2 mol% PMZT film is shown.

The different trap energy levels seen in Table 4 for PNZT and PNZT + 2 mol% PMZT films in the field up direction are consistent with a change in the hopping species in the most resistive part of

Table 4
Schottky barrier heights (SBH) and Poole-Frenkel trap energy level of PNZT films with/without a graded doping layer.

Film	Pristine		Degraded (300 kV/cm, 200°C, 23 hr)	
	SBH (eV) Field Up	SBH (eV) Field Down	PF Trap (eV) Field Up	PF Trap (eV) Field Down
PNZT	0.64 ± 0.09	0.46 ± 0.03	0.45 ± 0.01	0.65 ± 0.05
PNZT + 2 mol% PMZT	0.60 ± 0.01	0.69 ± 0.04	1.27 ± 0.03	0.59 ± 0.03

the films from Ti^{4+}/Ti^{3+} to $Mn^{4+}/Mn^{3+}/Mn^{2+}$ (Eq 5), after adding a PMZT top layer. The Mn concentration is lower than that of Ti, increasing the carrier hopping distance, causing a higher trap energy in the film and slowing down the electronic migration. It indicates that the PMZT layer reduces the maximum electric field in the depletion region by trapping electrons [21,33], and so improves the long-term reliability of the film.

$$Mn_{Ti}^{X} + e' \rightarrow Mn_{Ti}' Mn_{Ti}' + e' \rightarrow Mn_{Ti}'' \quad (5)$$

To further understand how the PMZT layer enhances the long-term reliability of PNZT films, modulus spectroscopy was used to detect the bulk conduction mechanism [51], in pristine state PNZT, PNZT with 1 mol% PMZT top layer film, PNZT with 3mol% PMZT top layer film, pristine and degraded PNZT with 2 mol% PMZT top layer films. Fig. 5 shows the measurements for the case in which the PMZT layer was on the cathode side. As seen in Fig. 5(a), only one peak is observed, which indicates a narrow distribution of conductivities and implies that defects, like oxygen vacancies, are homogenously distributed. The activation energy of the modulus peak detected in pristine PNZT film is 1.46 ± 0.01 eV, which is related to hole migration between V_{Pb}'' [52,53]

In contrast to the data of pristine PNZT films, the imaginary modulus spectroscopy of the pristine PNZT with a PMZT top layer consist of two or three peaks (Fig. 5 (b), (c), (d)), indicating the presence of different regions with different conductivities. The multiple modulus peaks also suggest that the PNZT and PMZT layers are electrically connected in series [40,54]. The calculated activation energy of the low frequency modulus peak (Peak 1) for all three PNZT with PMZT was around 1.45 ± 0.01 eV, which is also related to hole migration between V_{Pb}''. This activation energy was found to be independent of the Mn doping concentration, and was similar to that in the pristine PNZT film [53]. The higher frequency modulus peaks should relate to the higher conductivity Mn-doped top layer. For the PNZT with 2 mol% PMZT top layer film, the activation energies of the medium and high frequency peaks are 1.13 ± 0.02 eV and 1.04 ± 0.06 eV, respectively. For samples in which the Mn doping concentration was 3 mol%, there is only one peak at high frequency with the activation energy 0.61 ± 0.01 eV. The activation energy change suggests that the charge transport mechanism changed from hole migration between V_{Pb}'' to hole hopping/trapping between Mn ions [51-53] as the Mn concentration increased in the top layer. With addition of the PMZT layer on the PNZT films, $Mn^{2+/3+}$ ions start to act as hole trapping sites, leading to enhancement in the electronic conduction.

Based on the combination of results from leakage current measurements, TEM EELS analysis, and imaginary modulus spectroscopy, it is proposed that PNZT film with PMZT as the cathode, formed different regions with different conductivities electrically

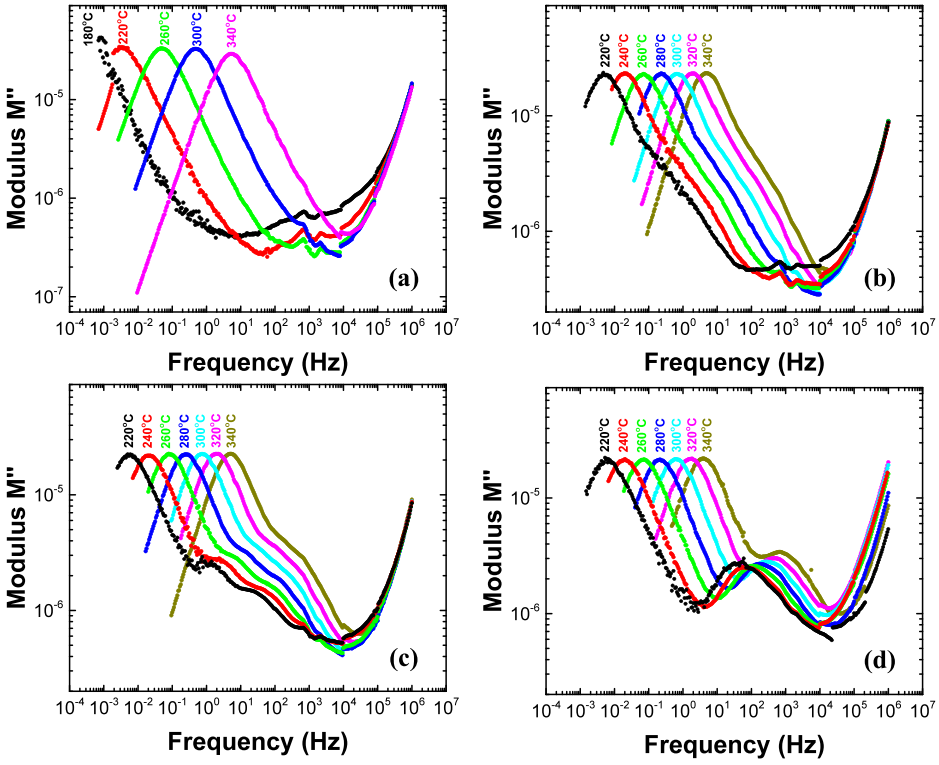

Fig. 5. Imaginary modulus plotted as a function of frequency at different temperatures measured on pristine state (a) PNZT film, (b) PNZT + 1mol% PMZT film, (c) PNZT + 2mol% PMZT film, (d) PNZT + 3mol% PMZT film.

connected in series. Addition of PMZT layers significantly increases the contribution of electronic conductivity to the total conductivity since Mn ions serve as charge hopping/trapping sites. In the degradation process of PNZT with PMZT layer film, the electrons trapping and hopping sites changed from Ti^{4+}/Ti^{3+} to $Mn^{4+}/Mn^{3+}/Mn^{2+}$, which increased the trapping energy level, decreased electron migration, reduced the maximum electric field in depletion layer and eliminated Ti ion reduction. Due to the combination of these factors, which induces a more uniform conductivity of the film, the long-term reliability of PNZT film with PMZT layer as the cathode greatly improved, resulting in dramatically increased film Highly Accelerated Lifetime Testing (HALT) lifetime values.

4. Conclusions

PNZT, PNZT with 1, 2, 3 mol% PMZT top layer (PNZT + x mol% PMZT), and PNZT with 1, 2 mol% PMZT seed layer (x mol% PMZT + PNZT) films with Zr:Ti ratio = 52:48 were deposited on platinized Si wafers by chemical solution deposition with commercial precursor solutions. All the films show similar dielectric and ferroelectric properties and comparable piezoelectric response. With the addition of a PMZT layer on the top or bottom of the films, the medium time to failure (t_{50}) in Highly Accelerated Lifetime Testing (HALT) under aggressive conditions (300 kV/cm, 200°C) shows a dramatic increase from 14.4 to 93.9 hours, or 27.7 to 94.6 hours, in the field up or field down polarity, respectively. In the degraded state, the conduction mechanism of PNZT and PNZT + 2 mol% PMZT films are dominated by Poole-Frenkel emission. The trap energy level is 0.45 ± 0.01, 1.27 ± 0.03 eV when measured in the field up direction; they have similar trap energy levels in the field down direction. In the TEM EELS data, PNZT films shows Ti reduction in the top layer after degradation. However, degraded PNZT + 2 mol% PMZT films do not show Ti reduction. These data suggest that the trapping sites of the electrons change from Ti ions to Mn ions after the addition of 2 mol% PMZT top layer on the cathode side. This slows down electron migration in the film and slows down degradation of the PNZT film. According to the imaginary modulus spectroscopy data, PNZT and PMZT layers are electrically connected in series. In PNZT with PMZT layer films, Mn ions starts to contribute to the electronic conduction (in addition to lead vacancies and $Pb^{2+/3+}$ hopping/trapping sites). Thus, adding a PMZT layer with a suitable doping concentration and thickness on the cathode end of the PNZT film could greatly increase film lifetime, without obvious degradation of its ferroelectric and piezoelectric properties.

Declaration of Competing Interest

The authors declare that they have no known competing financial interests or personal relationships that could have appeared to influence the work reported in this paper.

Acknowledgements

The authors are thankful to Professors Clive Randall and Michael Lanagan for their valuable discussions. Dr. Wei Luo's help in data fitting and analysis is gratefully acknowledged. Finally, the authors are very appreciative of support for this research from Xaar plc; the National Science Foundation, as part of the Center for Dielectrics and Piezoelectrics under Grant IIP-1841453 and IIP-1841466.

Supplementary materials

Supplementary material associated with this article can be found, in the online version, at doi:10.1016/j.actamat.2021.117251.

References

[1] J.S. Pulskamp, R.G. Polcawich, R.Q. Rudy, S.S. Bedair, R.M. Proie, T. Ivanov, G.L. Smith, Piezoelectric PZT MEMS technologies for small-scale robotics and RF applications, MRS Bull. 37 (2012) 1062–1070.
[2] P. Muralt, R.G. Polcawich, S. Trolier-McKinstry, Piezoelectric thin films for sensors, actuators, and energy harvesting, MRS Bull. 34 (2009) 658–664.
[3] Y. Miyazawa, H. Omae, T. Ishii, H. Koto, and F. Akahane, Seiko Epson Corp, United States Patent, US5113204A.
[4] N. Ledermann, P. Muralt, J. Baborowski, S. Gentil, K. Mukati, M. Cantoni, A. Seifert, N. Setter, {100}- textured piezoelectric $Pb(Zr_x, Ti_{1-x})O_3$ thin films for MEMS: integration, deposition and properties, Sens. Actuat. Phys. 105 (2003) 162–170.
[5] S. Trolier-McKinstry, P. Muralt, Thin film piezoelectrics for MEMS, J. Electroceramics 12 (2004) 7–17.
[6] W. Zhu, W. Ren, H. Xin, P. Shi, X. Wu, Enhanced ferroelectric properties of highly (100) oriented $Pb(Zr_{0.52}Ti_{0.48})O_3$ thick films prepared by chemical solution deposition, J. Adv. Dielectr. 3 (2013) 135011.
[7] B. Jaffe, W.R. Cook, H. Jaffe, Piezoelectric Ceramics, Academic Press Inc., 1971 London.
[8] Q.M. Zhang, J. Zhao, K. Uchino, J. Zheng, Change of the weak field properties of $Pb(ZrTi)O_3$ piezoceramics with compressive uniaxial stresses and its links to the effect of dopants on the stability of the polarizations in the materials, J. Mater. Res. 12 (1997) 226–234.
[9] T.R. Shrout, Innovations in Piezoelectric Materials for Ultrasound Transducers, Proc. 17th IEEE ISAF 3 (2008) 1–4.
[10] G.H. Haertling, C.E. Land, Hot-pressed $(Pb,La)(Zr,Ti)O_3$ ferroelectric ceramics for electrooptic applications, J. Am. Ceram. Soc. 54 (1971) 1–11.
[11] R. Gerson, Variation in ferroelectric characteristics of lead zirconate titanate ceramics due to minor chemical modifications, J. Appl. Phys. 31 (1960) 188–194.
[12] W. Zhu, I. Fujii, W. Ren, S. Trolier-McKinstry, Domain wall motion in A and B site donor-doped $Pb(Zr_{0.52}Ti_{0.48})O_3$ films, J. Am. Ceram. Soc. 95 (2012) 2906–2913.
[13] X.L. Zhang, Z.X. Chen, L.E. Cross, W.A. Schulze, Dielectric and piezoelectric properties of modified lead titanate zirconate ceramics from 4.2 to 300 K, J. Mater. Sci. 18 (1983) 968–972.
[14] W. Zhu, I. Fujii, W. Ren, S. Trolier-McKinstry, Influence of Mn doping on domain wall motion in $Pb(Zr_{0.52}Ti_{0.48})O_3$ films, J. Appl. Phys. 109 (2011) 064105.
[15] R.A. Eichel, P. Erhart, P. Traskelin, K. Albe, H. Kungl, M.J. Hoffmann, Defect-dipole formation in copper-doped $PbTiO_3$ ferroelectrics, Phys. Rev. Lett. 100 (2008) 095504.
[16] W.L. Warren, G.E. Pike, K. Vanheusden, D. Dimos, B.A. Tuttle, J. Robertson, Defect-dipole alignment and tetragonal strain in ferroelectrics, J. Appl. Phys. 79 (1996) 9250–9257.
[17] M.V. Raymond, D.M. Smyth, Defect chemistry and transport properties of $Pb(Zr_{1/2}Ti_{1/2})O_3$, Integr. Ferroelectr. 4 (1994) 145–154.
[18] J.F. Scott, K. Watanabe, A.J. Hartmann, R.N. Lamb, Device models for PZT/PT, BST/PT, SBT/PT, and SBT/BI ferroelectric memories, Ferroelectr 225 (1999) 83–90.
[19] S. Takatani, K. Kushida-Abdelghafar, H. Miki, Effect of H_2 Annealing on a $Pt/PbZr_xTi_{1-x}O_3$ interface studied by X-ray photoelectron spectroscopy, Jpn. J. Appl. Phys. 36 (1997) L435–L438.
[20] I.K. Yoo, S.B. Desu, J. Xing, Correlations among degradations in lead zirconate titanate thin film capacitors, Mater. Res. Soc. Proc. 310 (1993) 165–176.
[21] B. Akkopru-Akgun, W. Zhu, C.A. Randall, M.T. Lanagan, S. Trolier-McKinstry, Polarity dependent DC resistance degradation and electrical breakdown in Nb doped PZT films, Appl. Phys. Lett.: Mater. 7 (2019) 120901.
[22] R.M. Waser, Electrochemical boundary conditions for resistance degradation of doped alkaline-earth titanates, J. Am. Ceram. Soc. 72 (1989) 2234–2240.
[23] R. Waser, T. Baiatu, K.-H. Hardtl, dc electrical degradation of perovskite-type titanates: II single crystals, J. Am. Ceram. Soc. 73 (1990) 1654–1662.
[24] T. Baiatu, R. Waser, K.-H. Hardtl, dc electrical degradation of perovskite–type titanates: III a model for the degradation, J. Am. Ceram. Soc. 73 (1990) 1663–1673.
[25] W. Warren, K. Vanheusden, D. Dimos, G.E. Pike, B.A. Tuttle, Oxygen vacancy motion in perovskite oxides, J. Am. Ceram. Soc. 79 (1996) 536–538.
[26] R.V. Wang, P.C. McIntyre, ^{18}O tracer diffusion in $Pb(Zr, Ti)O_3$ thin films: A probe of local oxygen vacancy concentration, J. Appl. Phys. 97 (2005) 023508.
[27] D.M. Smyth, Defect structure in perovskite titanates, Curr. Opin. Solid State Mater. Sci. 1 (1996) 692–697.
[28] S.W. Ko, W. Zhu, C. Fragkiadakis, T. Borman, K. Wang, P. Mardilovich, S. Trolier-McKinstry, Improvement of reliability and dielectric breakdown strength of Nb-doped lead zirconate titanate films via microstructure control of seed, J. Am. Ceram. Soc. 102 (2019) 1211–1217.
[29] R. Waser, T. Baiatu, K. Härdtl, Degradation of dielectric ceramics, Mater. Sci. Eng. A 109 (1989) 171–182.
[30] R. Waser, T. Baiatu, K.H. Hardtl, dc electrical degradation of perovskite-type titanates: I, ceramics, J. Am. Ceram. Soc. 73 (1990) 1645–1653.
[31] J-S Yang, Y.S. Kang, I. Kang, S.M. Lim, S.-J. Shin, J.W. Lee, K.H. Hur, Comparison of the thermal degradation of heavily Nb-Doped and normal PZT thin films, IEEE T. Ultrasonic. Ferr. 64 (2017) 617–622.
[32] M.T. Chentir, E. Bouyssou, L. Ventura, G. Guégan, C. Anceau, Electrical Characterization and Reliability of Lanthanum Doped PZT Thin Films Capacitors, Integr. Ferroelectr. 96 (2008) 75–81.
[33] B. Akkopru-Akgun, T. Bayer, K. Tsuji, C.A. Randall, M.T. Lanagan, S. Trolier-M-

cKinstry, The influence of Mn doping on the leakage current mechanisms and resistance degradation behavior in lead zirconate titanate (PZT) films, submitted to Acta Mater, 2021.
[34] R.-A. Eichel, Structural and dynamic properties of oxygen vacancies in perovskite oxides-analysis of defect chemistry by modern multi-frequency and pulsed EPR techniques, Phys. Chem. Chem. Phys. 13 (2011) 368–384.
[35] C.K. Kwok, S.B. Desu, Formation kinetics of $PbZr_xTi_{1-x}O_3$ thin films, J. Mater. Res. 9 (1994) 1728–1733.
[36] B. Malic, M. Mandeljc, G. Drazic, M. Skarabot, I. Musevic, M. Kosec, Strategy for low-temperature crystallization of titanium-rich PZT thin films by chemical solution deposition, Integr. Ferroelectr. 100 (2008) 285–296.
[37] W. Zhu, T. Borman, K. Desaris, B. Truong, M.M. Lieu, S.W. Ko, P. Mardilovich, S. Trolier-McKinstry, Influence of PbO content on the dielectric failure of Nb–doped {100}-oriented lead zirconate titanate films, J. Am. Ceram. Soc. 102 (2019) 1734–1740.
[38] S. Sivaramakrishnan, P. Mardilovich, A. Mason, A. Roelofs, T. Schmitz-Kempen, S. Tiedke, Electrode size dependence of piezoelectric response of lead zirconate titanate thin films measured by double beam laser interferometry, Appl. Phys. Lett. 103 (2013) 132904.
[39] T.M. Borman, W. Zhu, K. Wang, S.W. Ko, P. Mardilovich, S. Trolier-McKinstry, Effect of lead content on the performance of niobium-doped {100} textured lead zirconate titanate films, J. Am. Ceram. Soc. 100 (2017) 3558–3567.
[40] J.J. Carter, T.J.M. Bayer, C.A. Randall, Degradation and recovery of iron doped barium titanate single crystals via modulus spectroscopy and thermally stimulated depolarization current, J. Appl. Phys. 121 (2017) 145106.
[41] R.G. Polcawich, C. Feng, P. Vanatta, R. Piekarz, S. Trolier-McKinstry, M. Dubey, M. Ervin, Highly accelerated lifetime testing (HALT) of lead zirconate titanate (PZT) thin films, in: Proc. 12th IEEE ISAF, 1, 2000, pp. 357–360.
[42] W. Zhu, B. Akkopru-Akgun, S. Trolier-McKinstry, Highly accelerated lifetime testing of potassium sodium niobate thin films, Appl. Phys. Lett. 111 (2017) 212903.
[43] M. Ohring, The Materials Science of Thin Films, Academic Press, 1992 London.
[44] F.-C. Chiu, A review on conduction mechanisms in dielectric films, Adv. Mater. Sci. Eng. (2014) 1–18 2014.
[45] R.E. Newnham, Properties of Materials: Anisotropy, Symmetry, Structure, Oxford University Press, 2004 Oxford.
[46] G.Y. Yang, E.C. Dickey, C.A. Randall, D.E. Barber, P. Pinceloup, M.A. Henderson, R.A. Hill, J.J. Beeson, D.J. Skamser, Oxygen nonstoichiometry and dielectric evolution of $BaTiO_3$ Part I-improvement of insulation resistance with reoxidation, J. Appl. Phys. 96 (2004) 7492–7499.
[47] G.Y. Yang, E.C. Dickey, C.A. Randall, D.E. Barber, P. Pinceloup, M.A. Henderson, R.A. Hill, J.J. Beeson, D.J. Skamser, Oxygen nonstoichiometry and dielectric evolution of $BaTiO_3$ Part II-insulation resistance degradation under applied dc bias, J. Appl. Phys. 96 (2004) 7500–7508.
[48] J. Robertson, W. Warren, B. Tuttle, D. Dimos, D. Smyth, Shallow Pb^{3+} hole traps in lead zirconate titanate ferroelectrics, Appl. Phys. Lett. 63 (1993) 1519–1521.
[49] MDD Rodriguez, From the mining to the obtaining of ferroelectric ceramics, J. Powder Metall. Min. 6 (2017) 1000160.
[50] B.A. Wechsler, M.B. Klein, Thermodynamic point defect model of barium titanate and application to the photorefractive effect, J. Opt. Soc. B 5 (1988) 1711–1723.
[51] B. Akkopru-Akgun, The role of defect chemistry in DC resistance degradation of lead zirconate titanate thin films, Pennsylvania State University, 2019 Ph.D. Thesis.
[52] H.N. Al-Shareef, D. Dimos, Leakage and Reliability Characteristics of Lead Zirconate Titanate Thin-Film Capacitors, J. Am. Ceram. Soc. 80 (1997) 3127–3132.
[53] J. Dih, R.M. Fulrath, Electrical conductivity in lead zirconate-titanate ceramics, J. Am. Ceram. Soc. 61 (1978) 448–451.
[54] T.J.M. Bayer, J.-J. Wang, J.J. Carter, A. Moballegh, J. Baker, D.L. Irving, E.C. Dickey, L.-Q. Chen, C.A. Randall, The relation of electrical conductivity profiles and modulus data using the example of STO: Fe single crystals: A path to improve the model of resistance degradation, Acta Mater. 117 (2016) 252–261.
[55] S. Sivaramakrishnan, P. Mardilovich, T. Schmitz-Kempen, S. Tiedke, Concurrent wafer-level measurement of longitudinal and transverse effective piezoelectric coefficients ($d_{33,f}$ and $e_{31,f}$) by double beam laser interferometry, J. Appl. Phys. 123 (2018) 014103.